Level set model for parallel folding of multilayered structures: comparisons with experiments

J. A. Boon C. J. Budd G. W. Hunt *,

Centre for Nonlinear Mechanics, University of Bath, Bath BA2 7AY

Abstract

Abstract goes here.

Key words:

1 Introduction

The folding of sedimentary rocks under tectonic compression has historically been of great interest to structural geologists, and subject to a number of different modelling perspectives (see for example Biot (1961) and Price and Cosgrove (1990)). It is often in the nature of such modelling processes that new questions lead to updates, and models can have a tendency to evolve. To provide benchmarks against which to verify such models, it is often useful to compare against simpler but readily quantifiable systems that can be tested experimentally, such as constrained and compressed layers of paper. Such comparisons have proved useful in the description of a number of naturally-occurring phenomena, including kink-banding (Wadee et al., 2004), and the focus of the present work – parallel folding (Budd et al., 2003).

One significant new addition to the analyst's armoury for such multilayered systems lies in level set theory (Osher and Sethian, 1988), which can express the geometry of the contacting folded layers in a natural but complete and rigorous manner. Whereas earlier models such as in Budd et al. (2003) and Edmunds et al. (2006) tend to rely on small-deflection assumptions ($4R_0^2 >>$

* Corresponding author
Email address: G.W.Hunt@bath.ac.uk (G. W. Hunt).

T^2 for example, where R_0 is the radius of curvature of the central interface of a folded region and T is the sample thickness), level set formulations are subject to no such restrictions (Boon et al., 2006). It is clear from experiments (for example Fig. 1) that such assumptions are violated with thick samples undergoing large deflections. Accordingly, small deflection assumptions underestimate the bending energy on the inside of a folded region, where curvatures are high. It is also clear that, in attempting comparisons of load-deflection response between model and experiments, such regions would be of major importance. It is for such reasons that we are presenting here a new set of comparisons for a level set model of parallel folding, updating that of Boon et al. (2006), against a new and carefully compiled set of experiments.

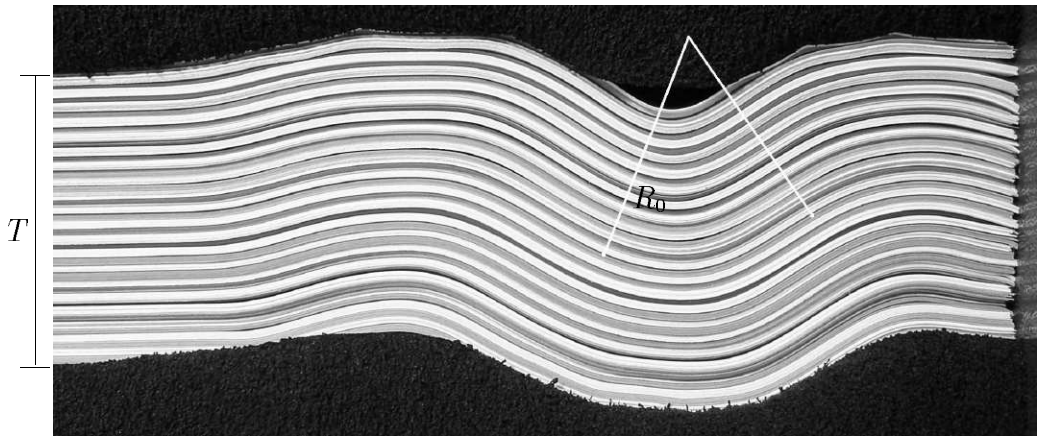

Fig. 1. In this experiment the radius of curvature of the central layer (R_0) is less than the thickness and therefore $4R_0^2 \gg T^2$ does not hold.

More explicitly, the small-deflection curvature assumption of Edmunds *et al* has the effect of omitting an important stiffening mechanism related to the tightening of the layers on the inside of a fold, that will limit its growth in amplitude. The experiments clearly indicated that some such mechanism was in place, and it was assumed at the time to be related to the compressive response of the foundation or bedding material. We show here that such a mechanism, although present, is not strong enough to restabilize the response at a load level commensurate with that seen experimentally. Instead, the level set model shows that amplitude of deformation is limited by a singularity on the inside of a fold, where the bending energy locally becomes infinite. Acting as the only restabiliizer, the corresponding nonlinear terms give results that compare well with the experiments, both in terms of what is seen physically and on plots of load against end-shortening.

2 Experiments

A set of 11 experiments on different examples of layered samples were conducted in the Department of Civil and Environmental Engineering at Imperial College London using the same rig as Wadee et al. (2004); Edmunds et al. (2006). Stacks of n half sheets of A4 paper (105 mm x 297 mm), alternating ten white with ten coloured, were placed between soft foam foundations top and bottom, as shown in Fig. 2. A vertical *overburden pressure* q per unit length

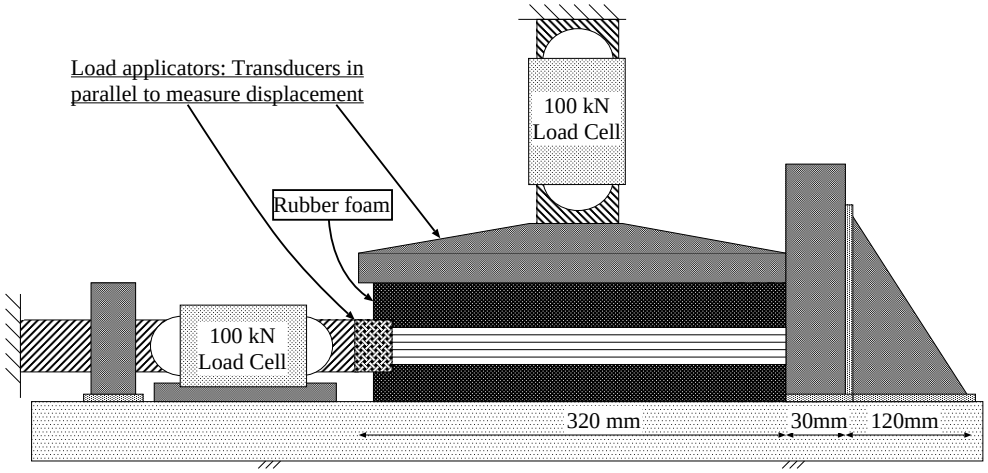

Fig. 2. Experimental rig. (After Edmunds et al. (2006))

was introduced via a rigid screw device, and a longitudinal axial load P was then applied at a constant (slow) rate via a second motorized load applicator. Both lateral and axial loads were measured using load cells as indicated, and displacement transducers recorded their movements. Readings were taken at 1 second intervals.

This set of experiments is subjected to the same load and displacement constraints as in Edmunds et al. (2006)'s experiments, namely that the rate of axial loading must be slow enough to be at least quasi-static and the overburden pressures must be moderate otherwise kink bands could form instead of parallel folds. Moreover, the thickness of the foam should be large enough to stop the rigid (outside) boundaries affecting the buckling process. Ramberg (1961) suggests that this should at least be the same order as the wavelength of the buckle. In view of the uncertainty in the earlier experiments over the stiffening effect of the foundation, and to accommodate thicker multilayer samples, foundations top and bottom of twice the thickness of those reported in Edmunds et al. (2006) were used (approximately 50 mm top and bottom in the present case).

The main characteristics of the experiments can be summarised as follows:

(1) Initial buckling typically occurred as a single hump at either the loaded (plunger) or the unloaded (reactive) end of the rig. It seemed to initiate with about equal likelihood at either end.
(2) After the initial instability there were significant differences in the post-buckling behaviour. A fold forming at the loaded end tended to deform locally without spreading along the length, see Fig. 3a, while one forming at the reactive end would initiate a sequence of so-called serial folds (Hunt et al., 2006), as seen in Fig. 4a.
(3) Load to corresponding deflection plots for these two instabilities showed considerably greater relative drop in load when buckling initiates at the loaded, rather than the reactive end, as seen when comparing Fig. 3b with Fig. 4b .
(4) In one case, after an initial instability at the reactive end, rather than a serial sequence forming, the next hump formed at the loaded end. This is shown in Fig. 5.

Much of this phenomenology seems to be a result of axial friction between the layered sample and the foundation (or shearing in the foundation itself which would have much the same effect). Before buckling, the load is clearly transmitted through the sample without significant reduction, as evidenced by point 1) above. However, after the initial hump forms, this is no longer the case. Remembering that load is measured at the point where it is applied, if the buckle initiates at the reactive end the load cell will record a combination of load at the hump, and friction from the foundation; thus the output of Fig. 4b shows evidence of a stick-slip sequence. If the initial instability and consequent drop in load themselves are taken as being much the same wherever the buckle forms, point 3) above confirms this frictional effect. Moreover, point 4) can supply an estimate of its magnitude. A further estimate of the effect of friction can be obtained by measuring the sudden drop in load that occurs as a serial sequence becomes fully formed. As this happens the load cell goes from measuring the load at the buckle and the friction with the foundation to measuring only the load at the buckle.

Although friction between layers is accounted for, friction between the layers and foundation has yet to be included in the mechanical model. If such friction is similarly felt over the length of the initial fold, so that the load at the loaded end of the hump is greater than that on the reactive side, this could also account for the fact that serial buckling only seems to propagate backwards, as described in point 2) above.

It is interesting to note that in contrast to Fig. 3 the output of Fig. 4 is more irregular, but the deflection pattern more ordered.

(a)

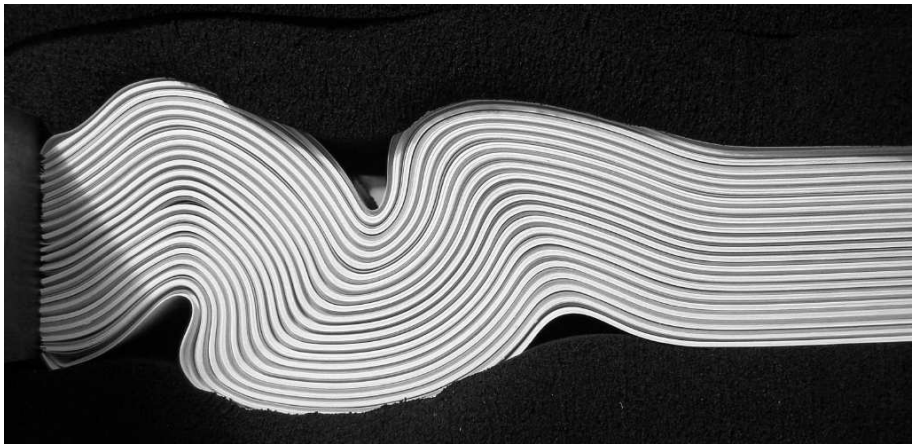

(b)

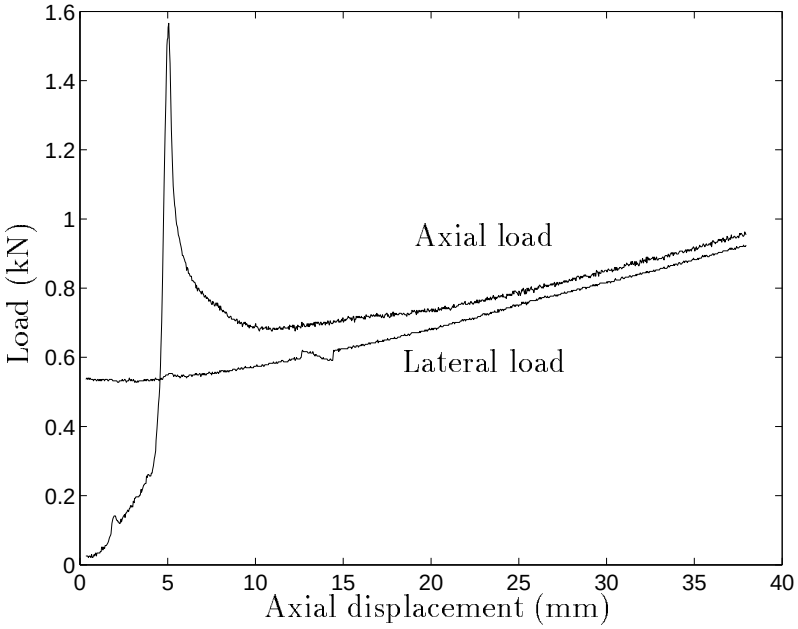

Fig. 3. First fold forming at the loaded end. (a) Pattern of deformation. (b) Axial and lateral loads, plotted against axial end-shortening.

3 Nonlinear elastic frictional models

Budd et al. (2003) derived a two layer model containing expressions for the bending energy, the work done against friction, the work done by the load and the energy stored by the foundation. In deriving the bending energy and the frictional energy they made the entirely reasonable assumption that $\Delta t^2 \gg 4R_0^2$. The model was extend to an n layer formulation, in which case the

(a)

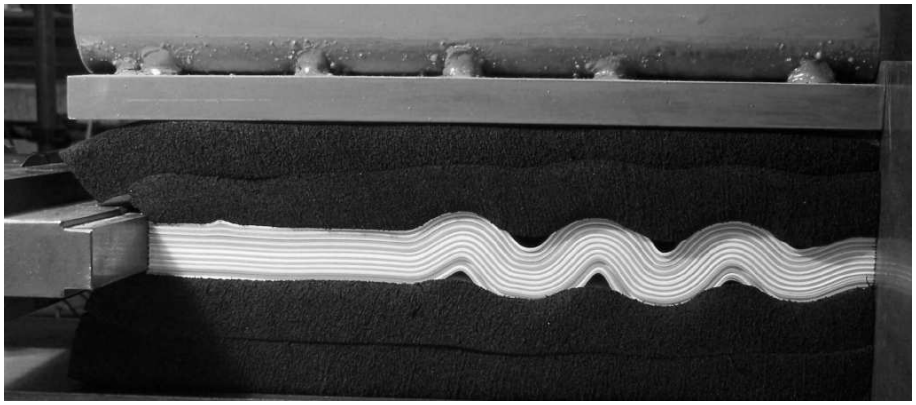

(b)

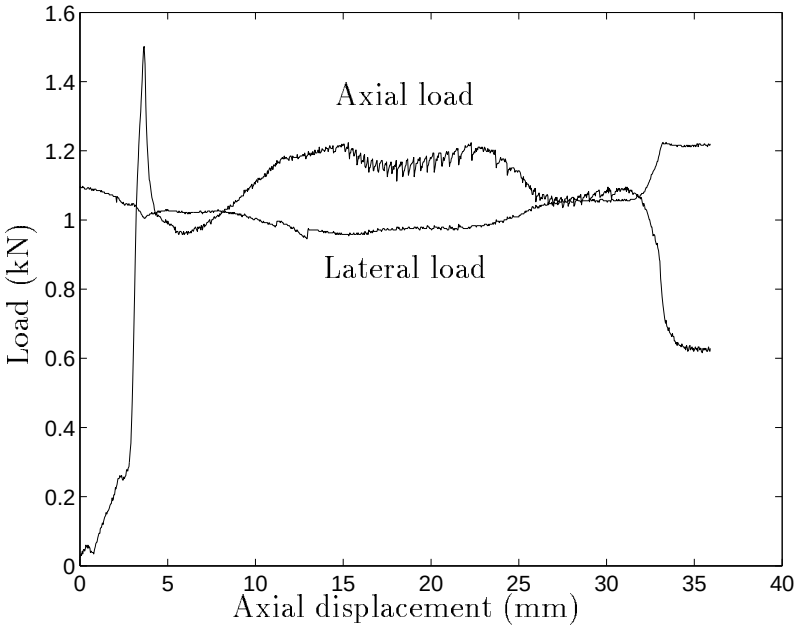

Fig. 4. First fold forming at the reactive end. (a) Pattern of deformation. (b) Axial and lateral loads, plotted against axial end-shortening.

bending energy becomes (Edmunds et al., 2006)

$$U_B = \frac{EIn}{2} \int_0^L \frac{\ddot{w}^2}{1 - \dot{w}^2} \, \mathrm{d}\sigma. \tag{1}$$

However, to arrive at this point the assumption is that $T^2 \gg \frac{4n^2 R_0^2}{(n-1)^2}$ or that $T^2 \gg 4R_0^2$ as $n \to \infty$. As the number of layers increases, this assumption is valid for ever decreasing deflections. As mentioned earlier, this is because the tightening of the layers on the inside of the fold dominates the bending energy of the whole mulitlayer. So until the geometry of the layers is well described, any mechanical model is bound to be inaccurate. These ideas motivated Boon et al. (2006) to look at front propagation techniques to describe the geometry of a multilayer. We now give a summary of their findings.

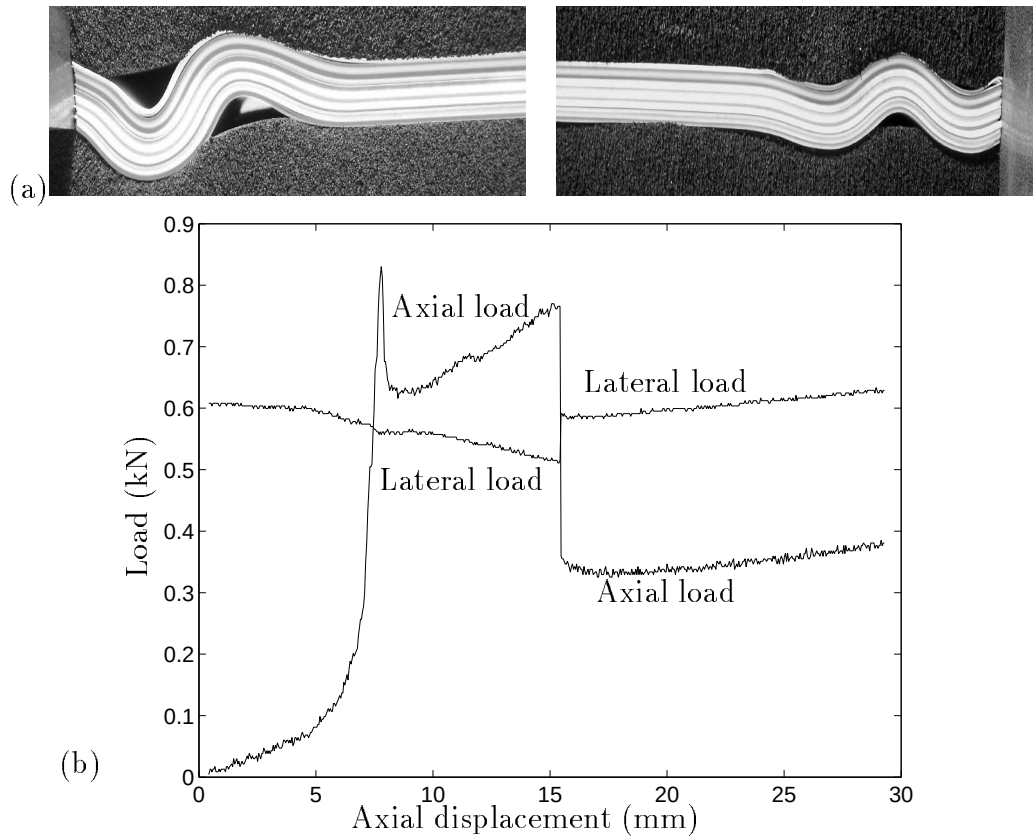

Fig. 5. Fold forms first at reactive end, and secondly at loaded end. (a) Pattern of deformation. (b) Axial and lateral loads, plotted against axial end-shortening.

3.1 Lagrangian represantaion of parallel folding

To describe the folding process we consider the set of curves $\Gamma_t : R^2 \to R^2$ so that $\Gamma_t = \{(x(s,t), y(s,t)) : s \in [0,1]\}$. The parallel folding assumption is that the *normal separation* between two curves parametrized by $t = t_1$ and $t = t_2$ is given by $|t_2 - t_1|$ and does not depend on s. This assumption leads to a simple construction of the *entire* set of curves for all t, given a reference curve for $t = 0$. The exact position of Γ_i at time t may be constructed by advancing each point of Γ_0 in its unit normal direction, $\mathbf{n}$, a distance $t = i\Delta t$ (Sethian 1999), where

$$\mathbf{n} = \frac{(-y_s^0, x_s^0)}{\sqrt{(x_s^0)^2 + (y_s^0)^2}}. \tag{2}$$

Here the suffix 0 refers to the reference curve. It follows from standard analysis that for each fixed $t = i\Delta t$ the Lagrangian description of Γ_t takes the form

$$\Gamma_t = \{(x(s,t), y(s,t)) = \left(\frac{-y_s^0 t}{((x_s^0)^2 + (y_s^0)^2)^{\frac{1}{2}}} + x^0(s), \frac{x_s^0 t}{((x_s^0)^2 + (y_s^0)^2)^{\frac{1}{2}}} + y^0(s) \right)\} \tag{3}$$

Equation (3) is valid for all $t = i\Delta t$, although the resulting curve may have points of singularity characterized by a lack of a well-defined normal vector.

We define T as the minimum radius of curvature along the reference curve as $T = \min(1/\kappa(s,0)) := 1/K$ where $\kappa(s,t)$ is the curvature. Whilst equation (3) and $t < T$ total arc-length of Γ_t is given by (Boon et al., 2006):

$$\sigma_t = \sigma_0 - t[\theta(s,0)]_{s=0}^{s=1} \tag{4}$$

A consequnce of this is that if $t < T$ and $[\theta(s,0)]_{s=0}^{s=1} = 0$, the total arc-length of each curve Γ_t remains constant. Conversely, if $t > T$ the reasoning breaks down and there is no gaurentee that the total arc-length is preserved.

3.1.1 Singularities

If $t > T$ the curve Γ_t has a singularity resulting in a self-intersecting curve with infinite curvature. This can be seen in Fig. 6 where a parabola is taken as the reference curve. Boon et al. (2006) show that as the singularity is approached

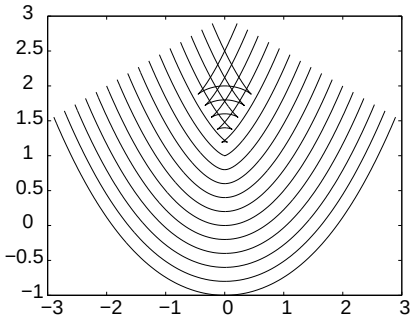

Fig. 6. Propagation of a parabolic reference curve Γ_0 showing the formation of the swallow-tail singularity

the second derivative, which is related to the curvature, can be written as $\mathrm{d}^2y/\mathrm{d}x^2 = K/\delta$ if $0 < \delta \ll 1$ is a small amount away from the singular point ($\delta = 1/K - t$).

3.2 Euler

The Euler representation aims to find the (x,y) equation of the curves Γ_i by looking at the differential equations governing the propagation of Γ as a function of t. We set $\Gamma_t = \{(x,y) : y = w(x,t)\}$. We suppose further that each set Γ_t occupies a part of a bounded, rectangular domain Ω in $\mathbb{R}^2$ extending from the left boundary of Ω to the right and separating Ω into two regions, Ω^-, the region *'inside'* the boundary and Ω^+, the region *'outside'* the boundary. We next assume that Γ_t is a *level set* of a higher dimensional function $\phi(x,y,t)$

so that

$$y = w(x,t) \quad \text{iff} \quad \phi(x,y,t) = 0.$$

The evolution of the function ϕ with t can then be linked to the propagation of the interfaces Γ_t.

Following the formulation of Sethian (1999), let $\mathbf{x}(t) = (x(t), y(t))$ be a point on the curve $\Gamma_t \equiv \{(x,y) : y = w(x,t)\}$. Starting from the identity $\phi(x,y,t) = 0$, it follows from the chain rule that,

$$\phi_t + \nabla\phi(\mathbf{x}(t),t) \cdot \mathbf{x}'(t) = 0, \tag{5}$$

where $\nabla\phi$ is defined to be (ϕ_x, ϕ_y). If $\mathbf{v}(x,y)$ is the speed in the normal direction, then $\mathbf{x}'(t) \cdot \mathbf{n} = v$, where the unit normal $\mathbf{n}$ is given by $\mathbf{n} = \nabla\phi/|\nabla\phi|$. It follows that ϕ satisfies the following hyperbolic partial differential equation of Hamilton–Jacobi type (the *level set equation*).

$$\phi_t + \mathbf{v}.|\nabla\phi| = 0. \tag{6}$$

Solving this equation for $\phi(x,y,t)$ together with a prescribed initial function $\phi(x,y,0)$ determines the curves $\Gamma_t = \{(x,y) \mid \phi(x,y,t) = 0\}$ and the exterior and interior regions:

$$\Omega_t^+ = \{(x,y) \mid \phi(x,y,t) > 0\} \quad \Omega_t^- = \{(x,y) \mid \phi(x,y,t) < 0\} \tag{7}$$

In the level set formulation, the condition for *parallel folding* is that the speed function, $\mathbf{v}(x,y)$ should be *constant*.

To solve the initial value problem we used the first order level set scheme (Osher and Sethian, 1988; Sethian, 1999). This method is able to handle singularities that can appear on when propagating past the radius of curvature of the reference layer.

3.3 Example of propagating a reference curve

Figure 7 shows the output from one of the experiments. Superimposed are dashed lines that give the level set position for various thickness. The thick curve in the middle of the multilayer is the reference layer which is found by fitting a cubic spline to points on the central layer.

Clearly the level set method is picking out the correct geometry of the multilayer throughout the sample.

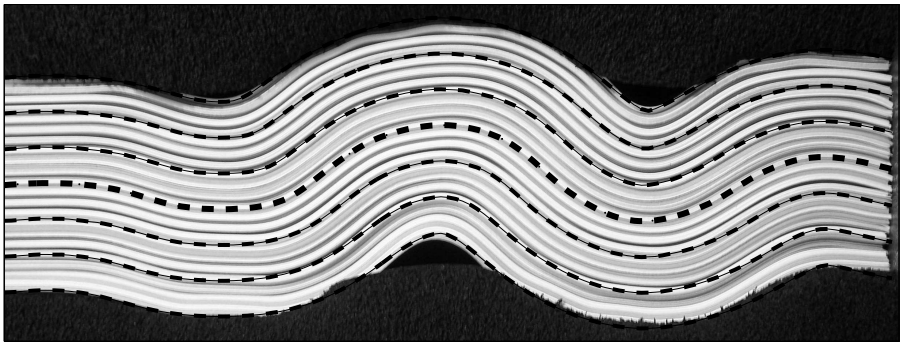

Fig. 7. Experimental output with level set curves superimposed. The thicker dashed line is the reference layer

4 Mechanics

4.1 Model description

We now derive the multilayer parallel folding model of Boon et al. (2006). Consider the geometry shown in Fig. 8, in which we assume that an initially undeformed multilayer material is compressed and buckled by an external load. This load is resisted by the stiffness of the layers, the frictional force as the layers slide in contact and the resistance of the matrix in which the layers are embeded. In the following models, we let x be the horizontal distance and σ the arc-length. The total length of each of the buckles is a constant L. We assume that there are $2n+1$ layers each of width Δt giving the material a total thickness of $T = (2n+1)\Delta t$. Let w_i, $i = -n \ldots n$ be the vertical deflection of the interface between two succesive layers.

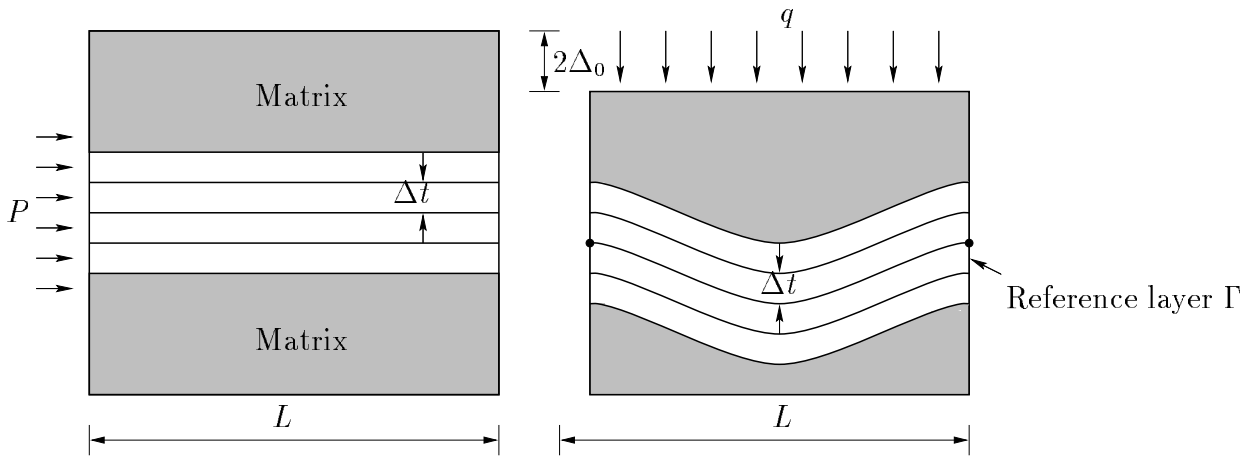

Fig. 8. The assumed geometry. The force q is applied before the force F. Δ_t is the layer thickness and L is the length of the fold. We assume that at the endpoints the angle of the layers with the horizontal is zero.

We now give the potential energy function V in terms of the level set function ϕ (Boon et al., 2006). The total potential energy comprises four components: V = Bending energy + Foundation energy − Work done by load + Work done against friction, or

$$V = U_B + U_F - P\mathcal{E} + \chi U_\mu \tag{8}$$

where function $\chi = \pm 1$ is the a *friction indicator* which ensures that fiction acts in the right direction during loading and unloading. We now give the expressions for the energy contributions. Let the letter i refer to the i^{th} interface between the layers and we use the notation $\phi^i(x,y) \equiv \phi(x,y,i\Delta t)$ where $\phi^i(x, w_i(x)) = 0$. Then

$$U_B = \frac{Eb\Delta t^3}{24} \sum_{i=-n}^{n} \int_{\Gamma_{i\Delta t}} \left(\nabla \cdot \frac{\nabla \phi^i}{|\nabla \phi^i|} \right)^2 \frac{|\nabla \phi^i|}{\phi^i_y} \, \mathrm{d}x \tag{9}$$

$$P\mathcal{E} = P \int_{\Gamma_{i\Delta t}} \left(1 + \left(\frac{\phi^0_y}{|\nabla \phi^0|} \right) \right) \frac{|\nabla \phi^0|}{\phi^0_y} \, \mathrm{d}x \tag{10}$$

$$U_\mu = \mu q \Delta t \sum_{i=-n}^{n} \int_{\Gamma_{i\Delta t}} \left| \sin^{-1} \left(\frac{\phi^i_x}{|\nabla \phi^i|} \right) \right| \frac{|\nabla \phi^i|}{\phi^i_y} \, \mathrm{d}x \tag{11}$$

$$U_F = \int_{\Gamma_{n\Delta t}} F(y_n) \frac{|\nabla \phi^n|}{\phi^n_y} - F(y_{-n}) \frac{|\nabla \phi^{-n}|}{\phi^{-n}_y} \, \mathrm{d}x \tag{12}$$

where b is the breadth of the paper and dots denote differentiation with respect to σ. In this expression the external matrix is assumed to have a Winkler force law, which receives a fuller explanation in section 6.3

5 Calculating the deformation profile

To determine the load of the multilayer material we must determine the stationary values of the energy functional and to make progress we make the approximation (Boon et al., 2006)

$$\Gamma_0 = \{(x,y) : y = w_0(\sigma) = Q \cos\left(\frac{\pi\sigma}{L}\right)\}. \tag{13}$$

When w is small the radius of curvature is large and this means that we can make the assumption $T^2 \gg 4R_0^2$ and we can consider the linearized potential

energy function (Edmunds et al., 2006) to enable us to find the critical load P^C and the length L. The energy function becomes

$$V = \int_0^L \left(\frac{Eb\Delta t^3}{24} \ddot{w}_0^2 - \frac{P}{2} \dot{w}_0^2 + \frac{K_1}{2} w_0^2 + \frac{(n-1)\chi\mu q T}{n} |\dot{w}_0| \right) \mathrm{d}\sigma. \tag{14}$$

A simple linear eigenvalue analysis yields the critical load

$$P^C = \frac{EIn\pi^2}{L^2} + \frac{K_1 L^2}{\pi^2}, \tag{15}$$

and minimising the critical load, with respect to the length L

$$L = \pi \left(\frac{EIn}{K_1} \right)^{\frac{1}{4}}. \tag{16}$$

The value of Q is fixed. Let $\mathcal{E}$, be the (horizontal) shortening of the interface due to the compressive load, found by the following Thompson and Hunt (1973)

$$\mathcal{E} = L - \int_0^L \sqrt{1 - w_\sigma^2}\, \mathrm{d}\sigma \tag{17}$$

where we drop the 0 from w_σ to ease the notation.

The level set problem is initialized by taking

$$\phi_{kj}^0 = y_k - Q \cos\left(\frac{\pi \sigma_j}{L} \right) \quad \text{with} \quad x_j - \int_0^{\sigma_j} \sqrt{1 - w_\sigma^2}\, \mathrm{d}\sigma = 0 \tag{18}$$

The linear dependence of the total energy on the (fixed) load P allows us to find P as a function of the single variable Q without solving nonlinear equations. In particular, setting $\partial V / \partial Q = 0$ we have simply

$$P = \frac{\partial U_B/\partial Q + \partial U_F/\partial Q + \chi \partial U_\mu/\partial Q}{\partial \mathcal{E}/\partial Q}. \tag{19}$$

For details on the numerical techniques used to solve these equations see Boon et al. (2006)

6 Comparison with experiments

In table 1 we present the quantities that are common to all 11 experiments. The remaining data which, is experiment specific is given in table 2. Direct comparison with the model requires independent estimates of E, q, μ, K_1 and K_3, obtained in the following manner.

Quantity	Value
a (mm)	297
b (mm)	105
Δt (mm)	0.1
E (kN/mm^2)	5
I (mm^4)	0.00875
K_3 (kN/mm^4)	3.49×10^{-7}

Table 1
Experimental quantities.

Expt	n	T (mm)	q (kN/mm)	P_L^* (kN)	Δ_L^* (mm)	K_1 (kN/mm^2)
1	120	12	0.0019	0.57	15.89	4.78×10^{-4}
2	120	12	0.0037	1.11	30.15	6.13×10^{-4}
3	120	12	0.0057	1.70	40.41	9.73×10^{-4}
4	220	22	0.0034	1.02	28.09	5.67×10^{-4}
5	220	22	0.0078	2.32	47.63	13.6×10^{-4}
6	320	32	0.0031	0.92	25.62	5.24×10^{-4}
7	320	32	0.0059	1.76	41.22	10.1×10^{-4}
8	320	32	0.0019	0.56	15.61	4.80×10^{-4}
9	420	42	0.0028	0.84	23.50	4.97×10^{-4}
10	420	42	0.0018	0.54	15.05	4.84×10^{-4}
11	420	42	0.0058	1.71	40.55	9.79×10^{-4}

Table 2
Experimental quantities.

6.1 Young's modulus and second moment of area

Wadee et al. (2004) and Edmunds et al. (2006) used the initial gradient of the $P - \mathcal{E}$ graph to estimate the in-line spring stiffness of the paper (stiffness of foundation is a number of orders of magnitude lower and can be neglected). Then the Young's modulus is simply

$$E = \frac{k_1 a}{Tb}, \tag{20}$$

where b and a are the breadth and length of the layers respectively and T is the total thickness of the sample.

Table 3 gives the average Young's modulus and the overburden pressure per

unit length that we obtained using this process and compares our findings with those presented by Wadee et al. (2004) and Edmunds et al. (2006). It is clear that as the overburden drops, so does the effective stiffness of the paper. We suspect that higher load levels surpress nonlinearities (such as the buckling of paper fibers) from having an impact. Whilst we appreciate that it is desirable to only use information gathered from the actual experiments we feel that given the uncertainty in the measurement and also the fact that bending will put a layer into both compression and tension, that it is acceptable to use a 'standard value' for the Young's modulus. For paper with a basis weight of 80 g/m^2 the mechanically measured Young's modulus (in tension) is 5 kN/mm^2 (Alava and Niskanen, 2006). This figure agrees well with compression tests performed with high loads (see table 3).

Paper	$\overline{E}$ (kN/mm^2)	$\overline{q}$ (kN/mm)
Wadee et al. (2004)	4.28	0.1
Edmunds et al. (2006)	1.45	0.01
Present paper	0.18	0.004

Table 3
Average Young's modulus $\overline{E}$ and the average overburden pressure $\overline{q}$ based on three sets of experiments performed on layers of paper.

The second moment of area for a single layer is given by

$$I = \frac{b\Delta t^3}{12}. \tag{21}$$

6.2 Overburden pressure and coefficient of friction

The overburden pressure per unit length, q, of the system is given by the lateral load at the first instability divided by the length of a layer a.

To find the coefficient of friction, μ, a stack of paper is inclined through an angle γ. The critical angle at which the paper begins to slip, γ^*, then determines μ (Wadee, 1999),

$$\mu = \tan\gamma^* \tag{22}$$

Since we were using the same paper as Wadee (1999), we have assumed a coefficient of $\mu = 0.57$ for our experiments.

A typical feature of energy based models is the difficulty that occurs when trying to estimate the *effective* stiffness of the foundation. This arises due to interactions between foundations lying above and below the multilayer and also the fact that there is a pre-compression in the form of the overburden pressure.

We assume an idealized nonlinear Winkler model for the foam based on a cellular descritpion (Hunt and Wadee, 1998). More explicitly, we assume the lateral load P_L gives a response that is initially linearly elastic, followed by a quadratic softening nonlinearity and a cubic restiffening nonlinearity (Edmunds et al., 2006). Thus

$$P_L = k_1\Delta_L - k_2\Delta_L^2 + k_3\Delta_L^3 \tag{23}$$

where $k_1 > k_2 > k_3 > 0$ and Δ_L is the lateral displacement.

We assume that the cellular model is valid over all deflections seen in the parallel folding experiments, including at the load when the first instability occurs. To find estimates for the foundation stiffnesses k_1, k_2 and k_3 we performed a set of four compression tests on the foam (in both loading and unloading). Fig. 9 shows the lateral load against lateral displacement plots of three of those experiments along with a least squares cubic fit. Since the curve fit is sensitive to the range of the data we fit a cubic over all the available data.

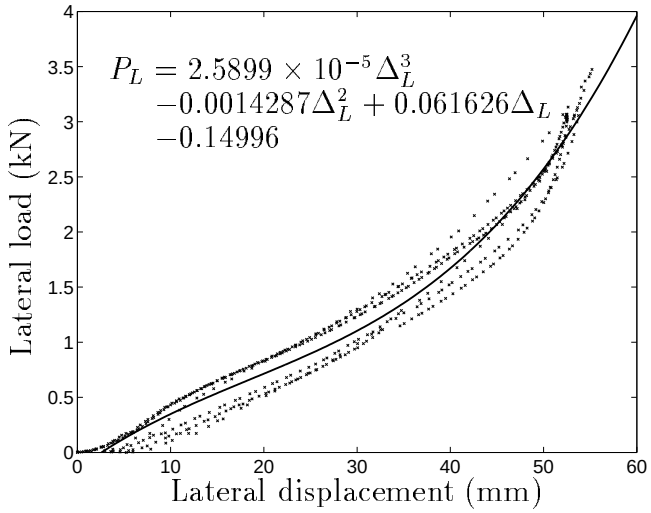

Fig. 9. Lateral compression and decompression tests performed on the foam subsequently used in the parallel folding experiments. The solid line is a cubic fit.

Now we account for the differences between the parallel folding experiments and the compression test on the foam. When the foam is used as a foundation in the parallel folding experiments it is first subjected to an overburden

pressure. With the level of overburden pressure applied in the experiments it means that any deflections of the paper into the foundation occur in the stiffened region of the foam's loading cycle. We set the point when the first instability occurs equal to (P_L^*, Δ_L^*) and shift the origin to this point so that

$$P_L - P_L^* = k_1'(\Delta_L - \Delta_L^*) - k_2'(\Delta_L - \Delta_L^*)^2 + k_3'(\Delta_L - \Delta_L^*)^3 \qquad (24)$$

This procedure provides the coefficients for the nonlinear stiffness of the foundation. We now show that due to symmetry the quadratic term has no effect on the energy stored in the foundation. To see this, we simplify the situation and assume that the parallel experiments consist of two springs and that under lateral loading P_L (Fig. 10(a)) the springs have each compressed a distance Δ_0 (Fig. 10(b)). Now let P be an axial load that causes the layers to move into one side of the foundation. Without loss of generality assume that the top layer moves into the foundation an amount δ_1 and the amount the bottom releases be a distance δ_2 (Figure 10(c)).

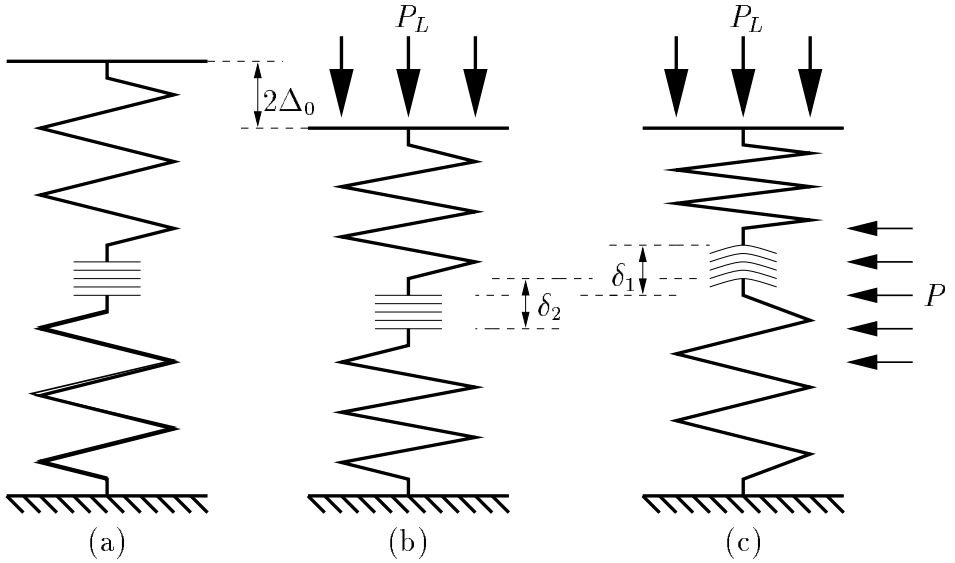

Fig. 10. The interaction of two springs acting either side of the layers when: (a) & (b) the pre-compression is added causing displacmenet Δ_0 in each spring and (c) the axial load forces one spring to compress by δ_1 and the other to decompress by δ_2.

When under extra compression δ_1, the first spring gives a positive energy contribution U_{F+}, which is calculated as

$$U_{F+} = \int_{\Delta_0}^{\Delta_0+\delta_1} \left(K_1\Delta + K_2\Delta^2 + K_3\Delta^3\right) \mathrm{d}\Delta \qquad (25)$$

As seen in Fig.11, in the process of rescaling the origin to the point of the first instability we also set $\Delta_0 = 0$ and hence

$$U_{F+} = \int_0^{\delta_1} \left(K_1\Delta + K_2\Delta^2 + K_3\Delta^3\right) \mathrm{d}\Delta = \frac{K_1}{2}\delta_1^2 + \frac{K_2}{3}\delta_1^3 + \frac{K_3}{4}\delta_1^4. \qquad (26)$$

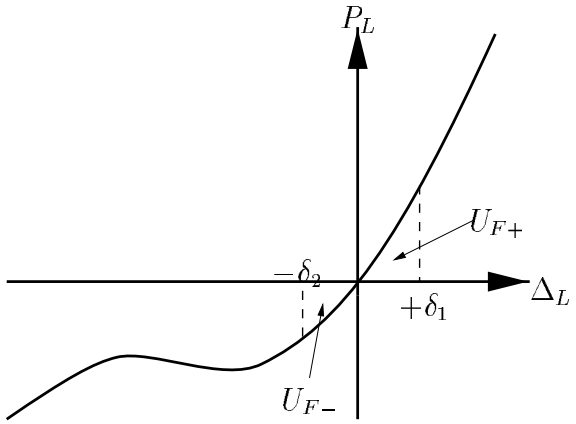

Fig. 11. Schematic of the $P_L - \Delta_L$ plot when increasing and releasing the pre-compression

The negative energy contribution U_{F-}, due to the second spring releasing δ_2 of its pre-compression is given by

$$U_{F-} = \int_{-\delta_2}^{0} \left(K_1\Delta + K_2\Delta^2 + K_3\Delta^3\right) \mathrm{d}\Delta = -\frac{K_1}{2}\delta_2^2 + \frac{K_2}{3}\delta_2^3 - \frac{K_3}{4}\delta_2^4. \quad (27)$$

The total energy is found by subtracting the negative energy contribution from the positive contribution

$$U_F = U_{F+} - U_{F-} = \frac{K_1}{2}(\delta_1^2 + \delta_2^2) + \frac{K_2}{3}(\delta_1^3 - \delta_2^3) + \frac{K_3}{4}(\delta_1^4 + \delta_2^4) \quad (28)$$

Now suppose that the top layer and the bottom layer are displaced by the same amount $\delta = \delta_1 = \delta_2$, which is reasonable for small deflections. In this case,

$$U_F = K_1\delta^2 + 0 * K_2 + \frac{K_3}{2}\delta^4 \quad (29)$$

We can see that the quadratic coefficient has no effect on the total energy of the foundation.

If one follows the reasoning of Edmunds et al. (2006) it is necessary to divide the coefficients of the fitted curve by the length a to get the stiffness per unit length of the foundation and also to multiply by 4 to account for two effects. The first is that the compression tests were on four layers compared to two in the paper experiments and the second is because in the foundation tests the foam layers were in series but act in parallel in the paper experiments.

$$K_1 = \frac{4k_1'}{a}, \quad K_2 = \frac{4k_2'}{a}, \quad K_3 = \frac{4k_3'}{a}. \quad (30)$$

This nonlinear hardening foundation provides a mechanism to enable the system to restabilize and lockup at some large value of $|Q|$. However, for the foam used in these experiments we found that the cubic restiffening term was not sufficiently large to account for the restabilisation and hence stick with a linear Winkler model (compare $K3$ & $K1$ in tables 1 & 2).

6.4 Comparisons

Theoretical wavelengths are caculated with equation (16) and are presented in table 4 along with experimental values that were obtained from measurement of photographs of the folds. Also in table 4 are the comparisons between the minimum load values $P_{\min}$ for the experiments where the first instability occured at the loaded end.

Expt	1	2	3	4	5	6	7	8	9	10	11
L_T	32.2	30.2	26.9	35.9	28.8	40.2	34.1	41.1	43.6	43.9	36.8
L_E	22.3	25.4	28.2	33.2	42.2	40.0	46.4	44.0	45.1	47.5	45.1
% Error	44.4	18.9	-4.6	8.1	-31.8	0.5	-26.5	-6.6	-3.3	-7.7	-18.4
$P_{T\,\min}$		0.21	0.29		0.81			0.53		0.77	1.60
$P_{E\,\min}$		0.45	0.53		0.95			0.56		0.68	1.35

Table 4
Comparison of theoretical (L_T) and experimental (L_E) wavelengths and the percentage error. Also shown are the theoretical ($P_{T\,\min}$) and experimental ($P_{E\,\min}$) values of the minimum load for experiments which buckled at the loaded end.

In the majority of the experiments there is a good agreement between the theoretical and the experimental wavelengths and the values of the percentage error appear evenly distributed about zero. The minimum load values are in excellent agreement for the experiments performed on thicker samples of paper, suggesting that the local increase in bending energy accounts for the restabilization. Figure 12(a) shows the experimental and theoretical axial loads against end-shortening of experiment 8. Also shown is a dashed line at the end-shortening when a singularity first appears in the outermost layer. We do not continue the theoretical curve to this line for two reasons. Firstly, it is unrealistic to expect the layers to form a sharp corner and instead it is much more likely that a second buckle would form (Hunt et al., 2006). Secondly, as we approach the singularity it becomes more difficult to accurately calculate the bending energy. This is due to the combination of the level set method artificially smoothing corners (Boon et al., 2006) and the difficulty in evaluating the equation (9) when a corner is present.

With the thinner samples (experiments 2 & 3) the predicted load is signifi-

(a) Experiment 8

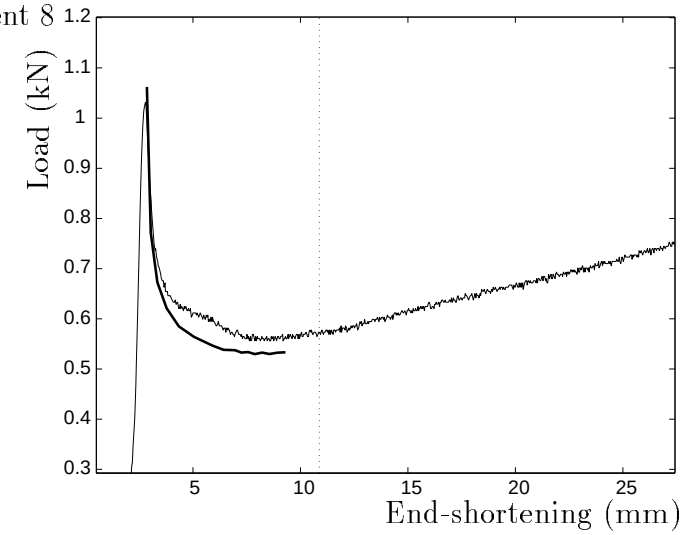

(b) Experiment 2

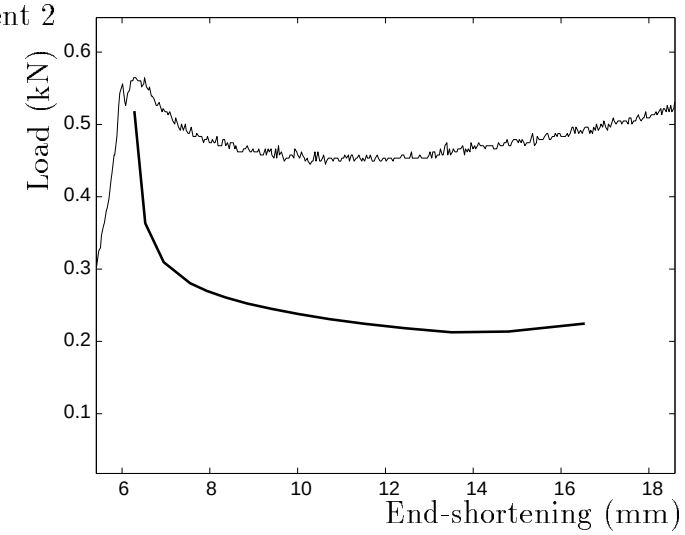

(c) Experiment 4

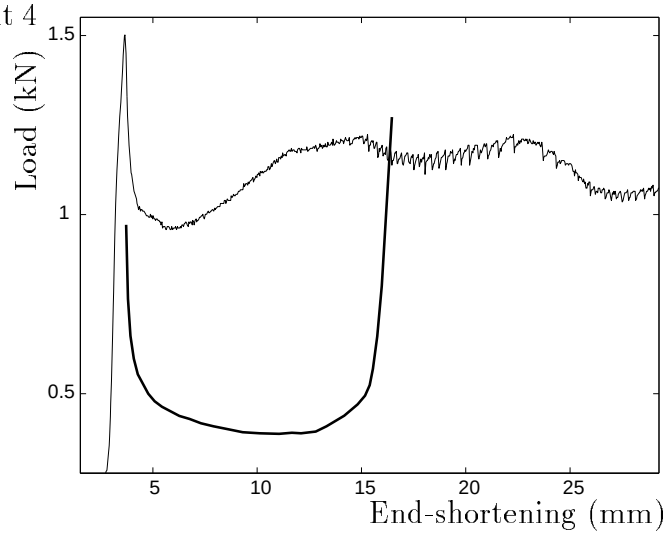

Fig. 12. Theoretical and experimental values of axial load against end-shortening for (a) thick sample that buckled from the loaded end (b) thin sample that buckled from the loaded end (c) buckled from the unloaded end.

cantly lower than the experimental load. We observe that in these experiments the axial load does not form a sharp peak as it buckles (see Fig. 12(b)) and an inspection of the initial buckle shows that the central layer is more of an S-shape (rather like a kink band (Wadee et al., 2004)) than sinusoidal when compared to the thicker samples (compare Figs. 13(a) & 13(b)). Also of importance for the thin samples is that the amplitude required to form a singularity is larger than the theoretical wavelength can deflect to (for large values of $|Q|$ (17) admits complex solutions).

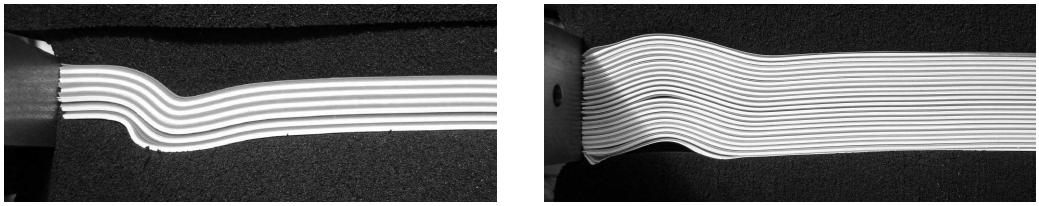

Fig. 13. The initial buckle of experiments 2 & 10 showing different mode shapes.

For completeness we include a plot of the axial load against end-shortening for an experiment that buckled from the loaded end and as predicted in section 2.1 the theoretical values are significantly lower than the experimental values (Fig. 12(c)).

7 Conclusions

The model presented here has compared well with experiment and we have shown, at least for the thicker samples, that the nonlinear bending energy forces the system to restabilize without the need for stiffening foundation models. However, there remain plenty of unanswered questions for the furture. It would be most interesting to perform the experiments with load cells at both the loaded and the unloaded ends to investigate further the shearing effect of the foundation. With our theory we are able to input different shapes for the reference layer, including an S-shape. Although presently, we have no explanation for why the thinner sample should adopt a different shape from the thicker samples and we should be careful when drawing generalized conclusions from a set of 11 experiments.

Acknowledgments

The authors would like to thank Dr Wadee for inviting us to Imperial College and for his advice in performing the experiments.

References

M. Alava and K. Niskanen. The physics of paper. *Rep. Prog. Phys.*, 69: 669–723, 2006.

M. A. Biot. Theory of folding of stratified viscoelastic media and its implications in tectonics and orogenesis. *Geol. Soc. Am. Bull*, 72:1595–1620, 1961.

J. A. Boon, C. J. Budd, and G. W. Hunt. Level set methods for the displacement of layered materials. *Proceedings of the Royal Society London A*, 2006.

C. J. Budd, R. Edmunds, and G. W. Hunt. A nonlinear model for parallel folding with friction. *Proc. R. Lond. A*, 459:2097–2119, June 2003.

R. Edmunds, G. W. Hunt, and M. A. Wadee. Parallel folding in multilayered structures. *J. Mech. Phys. Solids*, 54:384–400, 2006.

G. W. Hunt, R. Edmunds, C. J. Budd, and J. W. Cosgrove. Serial parallel folding with friction: a primative model using cubic B-splines. *J. Struct. Geol.*, 28:444–455, 2006.

G. W. Hunt and M. A. Wadee. Localization and mode interaction in sandwich structures. *Proc. R. Soc. Lond., A*, 454:1197–1216, 1998.

S. Osher and J. A. Sethian. Fronts propagating with curvature-dependent speed: Algorithms based on Hamilton–Jacobi formulations. *Journal of Computational Physics*, 79:12–49, 1988.

N. J. Price and J. W. Cosgrove. *Analysis of Geological Structures*. Cambridge University Press, Cambridge, UK, 1st edition, 1990.

H. Ramberg. Contact strain and folding instability of a multilayered body under compression. *Geol. Rundsch.*, 51:405–439, 1961.

J. A. Sethian. *Level Set Methods and Fast Marching Methods: Evolving interfaces in Computational Geometry, Fluid Mechanics, Computer Vision, and Materals Science*. Cambridge University Press, Cambridge, UK, 2nd edition, 1999.

J. M. T. Thompson and G. W. Hunt. *A general theory of elastic stability*. Wiley, London, 1st edition, 1973.

M. A. Wadee. Experimental evaluation of interactive buckle localization in compression sandwich panels. *J. Sandw. Struct. Mater.*, 1(3):230–254, 1999.

M. A. Wadee, G. W. Hunt, and M. A. Peletier. Kink band instability in layered structures. *J. Mech. Phys. Solids*, 52(5):1071–1091, 2004.